0.98 times that of neutral for the moderately stable case. These trends suggest greater vortical dispersion in an unstable atmosphere and less (or about the same) dispersion in a stable atmosphere, relative to neutral conditions.

Conclusions

Atmospheric stability effects in aircraft near-wake modeling can be simulated by vortical decay rates predicted by UNIWAKE. Inclusion of these effects into AGDISP and AgDRIFT will extend the capabilities of both models to handle general atmospheric conditions.

References

[1]Teske, M. E., Bilanin, A. J., and Barry, J. W., "Decay of Aircraft Vortices near the Ground," *AIAA Journal*, Vol. 31, No. 8, 1993, pp. 1531–1533.

[2]Bilanin, A. J., Teske, M. E., Barry, J. W., and Ekblad, R. B., "AGDISP: The Aircraft Spray Dispersion Model, Code Development and Experimental Validation," *Transactions of the American Society of Agricultural Engineers*, Vol. 32, No. 1, 1989, pp. 327–334.

[3]Teske, M. E., Bird, S. L., Esterly, D. M., Curbishley, T. B., Ray, S. L., and Perry, S. G., "AgDRIFT®: A Model for Estimating Near-Field Spray Drift from Aerial Applications," *Environmental Toxicology and Chemistry*, Vol. 21, No. 3, 2002, pp. 659–671.

[4]Bird, S. L., Perry, S. G., Ray, S. L., and Teske, M. E., "Evaluation of the AGDISP Aerial Spray Algorithms in the AgDRIFT® Model," *Environmental Toxicology and Chemistry*, Vol. 21, No. 3, 2002, pp. 672–681.

[5]Thistle, H. W., "The Role of Stability in Fine Droplet Dispersion in the Atmosphere: A Review of Physical Concepts," *Transactions of the American Society of Agricultural Engineers*, Vol. 43, No. 6, 2001, pp. 1409–1413.

[6]Bird, S. L., "A Compilation of Aerial Spray Drift Field Study Data for Low-Flight Agricultural Application of Pesticides," *Agrochemical Environmental Fate*, edited by M. L. Leng, E. M. K. Leovey, and P. L. Zubkoff, Lewis Publishers, Boca Raton, FL, 1995, pp. 195–207.

[7]Bird, S. L., Esterly, D. M., and Perry, S. G., "Off-Target Deposition of Pesticides from Agricultural Aerial Spray Applications," *Journal of Environmental Quality*, Vol. 25, No. 5, 1996, pp. 1095–1104.

[8]Panofsky, H. A., "Determination of Stress from Wind and Temperature Measurements," *Quarterly Journal of the Royal Meteorological Society*, Vol. 89, No. 1, 1963, pp. 85–94.

[9]Golder, D., "Relations Among Stability Parameters in the Surface Layer," *Boundary-Layer Meteorology*, Vol. 3, No. 1, 1972, pp. 47–58.

[10]Lewellen, W. S., and Teske, M. E., "Prediction of the Monin-Obukhov Similarity Functions from an Invariant Model of Turbulence," *Journal of the Atmospheric Sciences*, Vol. 30, No. 7, 1973, pp. 1340–1345.

[11]Donaldson, C. duP., "Construction of a Dynamic Model of the Prediction of Atmospheric Turbulence and the Dispersal of Atmospheric Pollutants," *American Meteorological Society Workshop on Micrometeorology*, edited by D. A. Haugen, Science Press, Boston, 1973, pp. 313–390.

[12]Bilanin, A. J., Teske, M. E., and Williamson, G. G., "Vortex Interactions and Decay in Aircraft Wakes," *AIAA Journal*, Vol. 15, No. 2, 1977, pp. 250–260.

[13]Bilanin, A. J., Teske, M. E., and Hirsh, J. E., "Neutral Atmospheric Effects on the Dissipation of Aircraft Vortex Wakes," *AIAA Journal*, Vol. 16, No. 9, 1978, pp. 956–961.

[14]Quackenbush, T. R., Teske, M. E., and Bilanin, A. J., "Computation of Wake/Exhaust Mixing Downstream of Advanced Transport Aircraft," AIAA Paper 93-2944, July 1993.

[15]Quackenbush, T. R., Teske, M. E., and Bilanin, A. J., "Dynamics of Exhaust Plume Entrainment in Aircraft Vortex Wakes," AIAA Paper 96-0747, Jan. 1996.

[16]Pasquill, F., "The Estimation of the Dispersion of Windborne Material," *Meteorological Magazine*, Vol. 90, No. 1, 1961, pp. 33–49.

[17]Bjorklund, J. R., Bowman, C. R., and Dumbauld, R. K., "User's Manual for the Mesoscale Wind Field Model Statistical Evaluation Computer Program MWMSE," H. E. Cramer, Inc., TR-84-347-01, Salt Lake City, UT, June 1984.

[18]Hecht, A. M., Bilanin, A. J., and Hirsh, J. E., "Turbulent Trailing Vortices in Stratified Fluids," *AIAA Journal*, Vol. 19, No. 6, 1981, pp. 691–698.

A. Plotkin
Associate Editor

One-Dimensional Numerical Study of Compressible Flow Ejector

Sam Han* and John Peddieson Jr.†
Tennessee Technological University, Cookeville, Tennessee 38505

Nomenclature

A	=	ejector mixing tube cross-sectional area, m^2
e	=	internal energy per unit mass, J/kg
M	=	Mach number
m'''_{inj}	=	primary flow mass injection rate per unit volume, kg/s · m^3
$\dot{m}$	=	mass flow rate, kg/s
p	=	static pressure, Pa
T	=	temperature, K
u	=	velocity, m/s

Subscripts

e	=	mixing tube exit
i	=	mixing tube inlet
inj	=	primary flow injection condition
p	=	primary flow
s	=	secondary flow
t	=	stagnation condition

Superscript

*	=	primary flow nozzle throat or previous iteration value

Introduction

COMPRESSIBLE flow ejectors are widely used in many engineering applications, and various analysis tools have been developed over the years to analyze them. The simplest approach is the control volume method, in which steady one-dimensional mass, momentum, and energy equations are used.[1–6] In control volume analysis, flow conditions are known only at the boundaries of an ejector, as shown in Fig. 1. There are four distinctive ejector flow regimes[1]: supersonic (S), saturated supersonic (SS), mixed (M), and mixed with separation (MS). In the S regime, the secondary flow is choked at a location c, which is called "Fabri or aerodynamic choking" (Fig. 1). In the SS regime, the secondary flow chokes at the area minimum in the secondary flow path. In the M regime, the secondary flow remains subsonic at the inlet, and there is no Fabri choking inside the mixing tube. In the MS regime, the primary flow stagnation pressure is so low that the primary flow separates in the diverging part of the primary flow nozzle. Fabri's model used four sets of equations covering the four flow regimes just discussed. Addy[2] extended Fabri's model further and developed more systematic methods of selecting these flow regimes. Another control-volume-based method assumes the exit flow Mach number and calculates the secondary flow inlet conditions by iteration.[6] In this approach, a critical assumption is the existence of static pressure equilibrium between the primary and the secondary flow somewhere downstream from the mixing tube inlet. The Fabri choking assumption is not used in this approach, and some researchers have pointed out that this method fails for cases in which the Fabri choking assumption is needed.[2]

Received 24 September 2001; revision received 19 February 2002; accepted for publication 8 April 2002.

*Professor, Department of Mechanical Engineering; shan@tntech.edu. Member AIAA.

†Professor, Department of Mechanical Engineering.

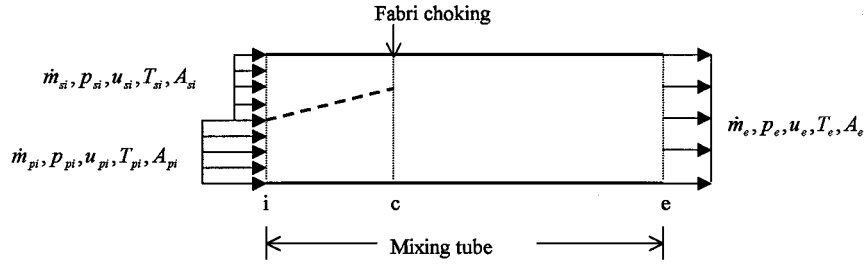

Fig. 1 Schematic of constant-area ejector mixing tube.

It is clear that control-volume-based analysis is suitable for fast parametric study of ejector performance but lacks physical insight into the mixing process. An alternative approach is one-dimensional numerical model, which provides some physics of interaction between the primary and secondary flow and is fast enough to be a practical design tool. The objective of the present study is to develop such a numerical model.

Numerical Model

Conservation of mass, linear momentum, and internal energy for one-dimensional transient compressible flow through a varying cross-sectional area yields

$$\frac{\partial \rho A}{\partial t} + \frac{\partial \rho u A}{\partial x} = m'''_{\text{inj}} A \tag{1}$$

$$\frac{\partial \rho u A}{\partial t} + \frac{\partial}{\partial x}\left[A\left\{\rho uu - \mu\frac{\partial u}{\partial x}\right\}\right] = -A\frac{\partial p}{\partial x} + m'''_{\text{inj}} A u_{\text{inj}} \tag{2}$$

$$\frac{\partial \rho e A}{\partial t} + \frac{\partial}{\partial x}\left[A\left\{\rho ue - \kappa\frac{\partial T}{\partial x}\right\}\right] = -p\frac{\partial uA}{\partial x} + m'''_{\text{inj}}\left(h_{\text{inj}} + 0.5^* x^2_{\text{inj}}\right)A \tag{3}$$

In Eqs. (1–3), x is the spatial coordinate, t time, μ dynamic viscosity, κ thermal conductivity, ρ density, and h enthalpy.

The numerical method used is a variant of SIMPLE.[7] Details of the SIMPLE methodology are well documented in the literature and are not repeated here except for the few modifications incorporated in the present model. The discretized momentum equation is[7]

$$\left(a^u_P/\alpha^u\right)u_P = a^u_E u_E + a^u_W u_W + \left(p^*_w - p^*_e\right)A_P + b^u + (1-\alpha^u)\left(a^u_P/\alpha^u\right)u^*_P + so^u/2 \tag{4}$$

where b^u includes the terms in the right-hand side of Eq. (2) except for the pressure gradient term. In Eq. (4), so^u is a term added to improve the approximation of momentum flux at the interface:

$$so^u = \left[\phi\left(r^+_e\right)\max(F_e, 0) + \phi\left(r^-_e\right)\max(-F_e, 0)\right]\left(u^*_P - u^*_E\right) + \left[\phi\left(r^-_w\right)\max(-F_w, 0) + \phi\left(r^+_w\right)\max(F_w, 0)\right]\left(u^*_P - u^*_W\right) \tag{5}$$

where

$$r^+_e = \left(u^*_P - u^*_W\right)/\left(u^*_E - u^*_W\right), \qquad r^-_e = \left(u^*_{EE} - u^*_E\right)/\left(u^*_E - u^*_P\right)$$

$$r^+_w = \left(u^*_W - u^*_{WW}\right)/\left(u^*_P - u^*_W\right), \qquad r^-_w = \left(u^*_E - u^*_P\right)/\left(u^*_P - u^*_W\right) \tag{6}$$

Depending on the choice of limiter function, $\phi(r)$, various numerical schemes can be represented,[8] for example, first order upwind

$$\phi(r) = 0 \tag{7a}$$

and Roe's Superbee

$$\phi(r) = \max[0, \min(2r, 1), \min(r, 2)] \tag{7b}$$

With $\phi(r) = 0$ and $so^u = 0$, Eq. (4) reduces to the original convection–diffusion formulation of the SIMPLE method. The discretized internal energy equation also contains a similar correction for the energy transport at the interface of control volumes.

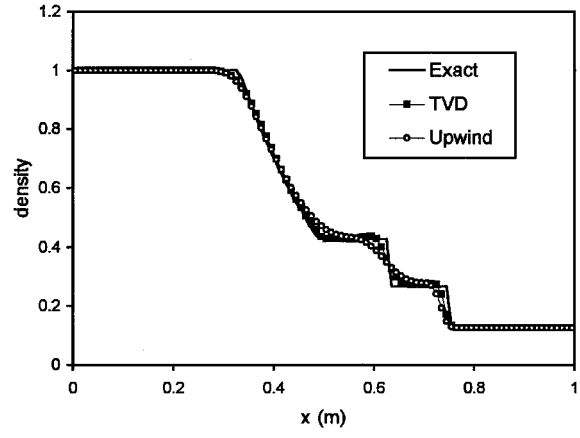

Fig. 2 Test shock tube problem: comparison of density distribution at $t = 0.14385$ s.

Mass conservation, expressed in terms of a pressure correction equation, is

$$a^p_p p'_p = a^p_E p'_E + a^p_W p'_W + b^p \tag{8}$$

where

$$a^p_E = \rho^*_e A^2_e \alpha^u / a^u_e + A_e \beta_e \max\left(-u^*_e, 0\right)$$

$$a^p_W = \rho^*_w A^2_w \alpha^u / a^u_w + A_w \beta_w \max\left(u^*_w, 0\right)$$

$$a^p_P = a^p_E + a^p_W + A_p \Delta x \beta_P / \Delta t$$

$$b^p = \left(-\rho^*_P A_P + \rho^0_P A^0_P\right)\Delta x/\Delta t - A_e \rho^*_e u^*_e + A_w \rho^*_w u^*_w + m'''_{\text{inj}} A \Delta x \tag{9}$$

In Eq. (9), β is related to the sonic speed in the flow, $\beta = 1/\gamma RT = 1/a^2$, and the density change is related to the pressure change by $\rho' = \beta p'$ (Ref. 9).

Figure 2 shows the accuracy of the proposed numerical method for a shock tube problem. As expected, a total variation diminishing (Roe's) scheme gives better resolution of the discontinuities and is used in the present study.

Comparisons with Test Data

Figure 3a is a schematic representation of an experimental ejector used in Ref. 1. The primary fluid is compressed air, and the secondary fluid is throttled air. The exit pressure at the end of the mixing tube is the atmospheric pressure. The stagnation temperatures of the primary and secondary flows are the atmospheric temperature.

Figure 3b shows the computational domain used to simulate Fabri's experimental ejector. The area of the flow passage in Fig. 3a is converted to a circular cross section with equivalent area in Fig. 3b. The boundary conditions used for the simulation are as follows. At $x = 0$, one dependent variable (velocity is chosen) is numerically calculated, and the remaining two dependent variables (temperature and density) are obtained by an isentropic expansion of the secondary flow reservoir conditions. At $x = L$, if the outflow is subsonic, the atmospheric static pressure is imposed as a

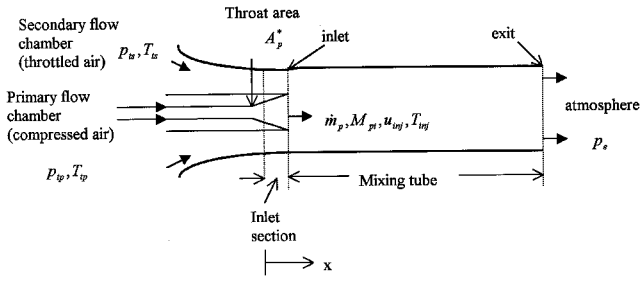

Fig. 3a Schematic of Fabri's experimental ejector.

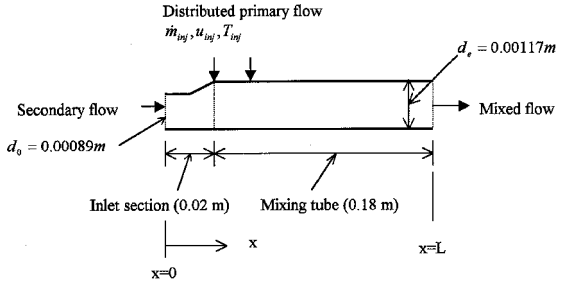

Fig. 3b One-dimensional computational domain.

required boundary condition and the temperature and the exit velocity are calculated numerically. If supersonic, all flow variables are extrapolated.

The primary flow effects enter the flowfield as source terms, which are independent of the flowfield in the system. The mass injection rate of the primary flow is fixed at the choked condition. The primary flow injection velocity and temperature, however, depend on the way the primary flow expands from the throat to the point where the primary flow enters the mixing tube. The first method is to assume that the primary flow expands isentropically according to the primary flow nozzle geometry. However, the experimental results in Ref. 1 showed that the primary flow expansion depends strongly on the primary-to-secondary stagnation pressure ratio at the inlet and the exit pressure at the end of mixing tube. In the second method, therefore, the primary flow is allowed to expand until it matches the secondary flow pressure at the inlet of the mixing tube. This approach is possible because the transient pressure in the entire system (inlet and mixing tube) is known from numerical calculation. Depending on the relative pressure, the primary flow, thus, can be over- or underexpanded in the second method.

Experimental results showed that the primary and secondary flow mixing occurs over an extended distance along the mixing tube, typically over a distance of approximately 10 times the diameter of the mixing tube. To simulate this mixing process, injection of the primary flow is distributed over the mixing tube. Mass injected by the primary flow is divided by the number of control volumes (covering up to 10 times the diameter of the mixing tube) and distributed as source terms in each control volume. The numerically predicted bypass ratio ($\dot{m}_s/\dot{m}_p$) does not change as long as the primary flow is introduced over several control volumes. If the primary flow is introduced in one or two control volumes, the sudden pressure increase due to the mass injection resulted in a normal shock for the secondary flow in certain cases. This is not usually observed in a well-designed compressible flow ejector.

The grid dependency of the numerical results in terms of the bypass ratio is tested by varying the number of control volumes in each of the inlet and the mixing tube sections. The bypass ratio was 0.308 (10×60), 0.327 (20×60), 0.326 (30×60), and 0.327 (20×80). Increasing the control volumes beyond 20×80 did not change the bypass ratio. A 20×80 control volume was selected for all subsequent simulations.

In Fig. 4, numerically predicted bypass ratios are compared with experimental data as a function of p_{ts}/p_e, when $p_{tp}/p_e = 5.5$. In Fig. 4, S, SS, and M indicate flow regimes as discussed earlier. There are two sets of numerical results in Fig. 4. One is obtained by the first method of the primary flow expansion, which gives

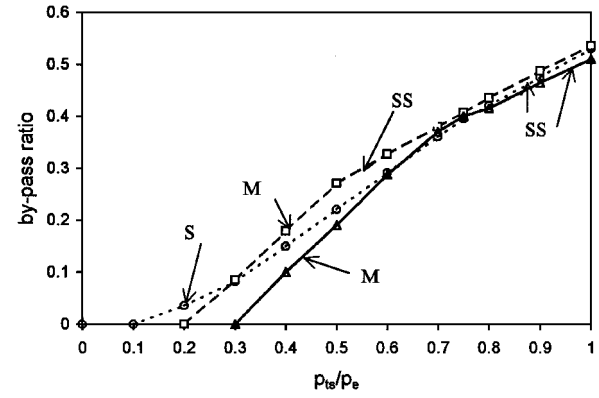

Fig. 4 Comparison of the bypass ratio: ○, test data; △, numerical data with the first method of the primary flow expansion; and □, numerical data with the second method of the primary flow expansion.

$M_{pi} = 1.78$. In this case, numerical results underestimate the secondary flow rate when the secondary flow stagnation pressure ratio is low ($p_{ts}/p_e < 0.6$). For higher secondary flow stagnation pressures ratio, the numerical results are in good agreement with the test data. The numerical results show that ejector flow is in the M regime up to $p_{ts}/p_e = 0.75$ and in the SS regime beyond. In the test data, the flow is in the S regime up to $p_{ts}/p_e = 0.75$ and in the SS regime beyond. Fabri choking in numerical results is interpreted as the mixed flow becomes sonic in the mixing tube (not in the inlet area minimum) while the inlet secondary flow remains subsonic. Numerical results did not show the Fabri choking for the given operating conditions.

The other set of numerical results is obtained by the second method of the primary flow expansion. It is found that the pressure at the first control volume where the primary flow injection begins ($x = 0.02$ m) is much lower than the primary flow nozzle exit pressure. Thus, the primary flow is allowed to expand further, and the primary flow velocity increases resulting in increased bypass ratio. The primary flow inlet Mach number M_{pi} increased from 1.78 to 2.06 when $p_{ts}/p_e = 0.3$ and to 1.95 when $p_{ts}/p_e = 0.8$. This indicates that when the secondary flow rate is small, the secondary flow pressure at the mixing tube inlet is low, resulting in increased primary flow speed. With the increased primary flow speed, the bypass ratio increases, and the agreement with test data is improved at lower secondary flow stagnation pressure ratios. Ejector flow remains in the M regime and transitions to the SS regime occurs at about $p_{ts}/p_e = 0.5$.

Conclusions

A one-dimensional numerical model is developed for the analysis of compressible constant-area ejectors. Numerical results are compared with experimental data in terms of the bypass ratio. The bypass ratio predicted by the numerical model agrees well with test data over a range of operating conditions except in cases in which the secondary flow stagnation pressure is extremely low. For such cases, the numerical model consistently underestimates the bypass ratio unless the primary flow is allowed to expand to match the pressure where it meets the secondary flow. One advantage of the present approach is that the secondary flow speed at the inlet of the mixing tube, M_{si}, is a part of numerical solution and need not be specified before the analysis as opposed to the control-volume-based analyses.

Acknowledgments

This research was supported by the Advanced Space Transportation Program Office, NASA Marshall Space Flight Center (MSFC), Grant NAG8-1794. The authors express their appreciation to John Hutt and John Blevins, MSFC, for their support and to the reviewers for their critical evaluation of the paper.

References

[1]Fabri, J., and Siestrunck, R., "Supersonic Air Ejectors," *Advances in Applied Mechanics*, Vol. 5, 1958, pp. 1–34.

[2]Addy, A. L., "The Analysis of Supersonic Ejector Systems," von Kármán Inst. for Fluid Dynamics, Lecture Ser. 79, April 1975.
[3]Emanuel, G., "Comparison of One-Dimensional Solutions with Fabri Theory for Ejectors," *Acta Mechanica*, Vol. 44, 1982, pp. 187–200.
[4]Alperin, M., and Wu, J., "Thrust Augmenting Ejectors, Part 1," *AIAA Journal*, Vol. 21, No. 10, 1983, pp. 1428–1436.
[5]Dutton, J. C., and Carroll, B. F., "Optimal Supersonic Ejector Designs," *Journal of Fluids Engineering*, Vol. 108, 1986, pp. 414–420.
[6]Heiser, W. H., and Pratt, D. T., *Hypersonic Airbreathing Propulsion*, AIAA Education Series, AIAA, Washington, DC, 1994, pp. 445–452.
[7]Patankar, S. V., *Numerical Heat Transfer and Fluid Flow*, Hemisphere, New York, 1980, Chap. 6.
[8]Przekwas, A. J., and Yang, H. Q., "Advanced Computational Fluid Dynamics Methodology for Fast Transients Encountered in Nonlinear Combustion Instability Problems," SBIR/NASA Marshall Space Flight Center Phase 1 Final Rept., Computational Fluid Dynamics Research Corp., Rept. 4065/1, Aug. 1989.
[9]Han, S., "A Generalized Implicit Finite Difference Method for Transient Analysis of Compressible and Incompressible Fluid Flows," *ASME Numerical Methods for Fluid Transient Analysis*, edited by C. S. Martin and M. H. Chaudhry, FED Vol. 4, American Society of Mechanical Engineers, Fairfield, NJ, 1983, pp. 17–21.

P. R. Bandyopadhyay
Associate Editor

Extension of a Method for Determination of Flight Equipment Acceleration

Romualdo Ruotolo*
Politecnico di Torino, 10129 Turin, Italy

Nomenclature

$\ddot{a}(\omega)$	=	input acceleration
C	=	number of components
$\{F_r\}$	=	reaction forces
$\{f\}$	=	excitation for the coupled structure
f_k, ω_k	=	hard-mounted natural frequency of kth component
$[K]$	=	stiffness matrix of secondary structure
k_k	=	stiffness of the connection between kth component and secondary structure
L_j	=	jth modal participation factor of coupled structure
$[l]$	=	modal participation factors of secondary structure
$[M]$	=	secondary structure mass matrix
$[M_c]$	=	mass matrix related to the components
$[\bar{M}_c]$	=	$[M_c]$ partitioned
m_k	=	mass of kth component
N	=	number of modes of the secondary structure
$\{q\}$	=	generalized coordinates of elastic modes
$\{q_r\}$	=	generalized coordinates of grounded nodes
r_j	=	generalized coordinate of the coupled structure
$S(\omega)$	=	input power spectral density
$[V_c]$	=	transformed mass matrix of components
$[\bar{V}_c]$	=	$[V_c]$ partitioned
$\{y\}$	=	degrees of freedom (DOF) of the secondary structure
$\{y_c\}$	=	displacements at the components' connection points
$\{y_i\}$	=	internal DOF of the secondary structure
$\{y_r\}$	=	grounded DOF of the secondary structure
$\{\delta\}$	=	components' relative displacements, $\{\delta_a\} - \{y_c\}$
$\{\delta_a\}$	=	components' absolute displacements
ζ	=	viscous damping ratio
$[\Lambda]$	=	eigenvalue matrix (diagonal) of the grounded secondary structure
σ_{δ_k}	=	standard deviation of the absolute acceleration of kth component
$[\Phi]$	=	mass normalized mode shapes of the secondary structure
$[\Phi_{rr}]$, $[\Phi_{ir}]$	=	translational matrices
$[\Psi]$	=	mass normalized mode shapes of the coupled structure
ω_j^2	=	jth eigenvalue of the coupled structure

Subscripts and Superscripts

c	=	component
i	=	ith internal DOF of the secondary structure
j	=	jth eigenmode of the coupled system
k	=	kth component
r	=	rth grounded DOF of the secondary structure

Introduction

DURING the launch, loads from different sources excite spacecraft primary and secondary structures. In particular, random oscillations of the primary structure, assumed known during the preliminary design, can be considered as a random vibration environment for secondary structures, for example, mounting frames. This excitation is of great importance for the determination of load factors acting on flight equipment, for example, electronic boxes, batteries, and scientific instruments, that are supported by secondary structures.

As described in Ref. 1, several techniques are used in engineering practice to evaluate the dynamic response of components, even though it has been demonstrated that some methods are too much conservative (in particular the technique based on the use of Miles's equation[2]). To obtain an accurate estimate of the acceleration of flight equipment, recently a new, highly cost-efficient technique has been proposed by Ruotolo and Cotterchio.[3] It has the main advantage of requiring only a few properties of the secondary structure to be grounded at the interface with the primary structure, so that it permits optimization runs aimed at mass saving.

Nevertheless, the formulation of the method described in Ref. 3 permits consideration of only a single piece of flight equipment connected to the secondary structure, so that its use is limited in practical applications. As a consequence, in this Note the technique is extended to deal with several components, permitting the consideration of real space structures, for example, nodes 2 and 3 of the International Space Station.

Determination of Components' Acceleration

Figure 1 shows a number of components connected to a secondary structure. It is assumed that stiffness and mass matrices of the latter structure are known so that its potential and kinetic energy can be written as

$$U_s = \tfrac{1}{2}\{y\}^T[K]\{y\}, \qquad T_s = \tfrac{1}{2}\{\dot{y}\}^T[M]\{\dot{y}\} \tag{1}$$

In the following discussion, it is assumed that the kth component is connected to only one degree of freedom (DOF) of the secondary structure through a spring with stiffness k_k. When all DOF of the connection points are collected into the vector $\{y_c\}$ and the relative displacement between components and corresponding mounting points on the secondary structure are introduced, potential and kinetic energies related to flight equipment are given by

$$U_c = \tfrac{1}{2}\{\delta\}^T[k_c]\{\delta\}, \qquad T_c = \tfrac{1}{2}(\{\dot{y}_c\} + \{\dot{\delta}\})^T[m_c](\{\dot{y}_c\} + \{\dot{\delta}\}) \tag{2}$$

where matrices $[k_c]$ and $[m_c]$ have rigidities k_k and masses m_k on their principal diagonal. When the corresponding energies

Received 3 November 2001; revision received 6 March 2002; accepted for publication 11 March 2002.

*Assistant Professor, Department of Aeronautical and Space Engineering, c.so Duca Abruzzi 24. Member AIAA.